1-25-1997

Beryllium Fluoride and Phalloidin Restore Polymerizability of a Mutant Yeast Actin (V266G,L267G) With Severely Decreased Hydrophobicity in a Subdomain 3/4 Loop

Bing Kuang
University of Iowa

Peter A. Ruhenstein
University of Iowa

Citation Information

Kuang, Bing; and Ruhenstein, Peter A.. 1997. Beryllium Fluoride and Phalloidin Restore Polymerizability of a Mutant Yeast Actin (V266G,L267G) With Severely Decreased Hydrophobicity in a Subdomain 3/4 Loop. *Journal of Biological Chemistry*. Vol.272(2). 1237-1247. https://doi.org/10.1074/jbc.272.2.1237 PMID: 8995427 ISSN: 0021-9258

Beryllium Fluoride and Phalloidin Restore Polymerizability of a Mutant Yeast Actin (V266G,L267G) With Severely Decreased Hydrophobicity in a Subdomain 3/4 Loop

THE JOURNAL OF BIOLOGICAL CHEMISTRY
Vol. 272, No. 2, Issue of January 10, pp. 1237–1247, 1997
Printed in U.S.A.

Beryllium Fluoride and Phalloidin Restore Polymerizability of a Mutant Yeast Actin (V266G,L267G) with Severely Decreased Hydrophobicity in a Subdomain 3/4 Loop*

(Received for publication, July 9, 1996, and in revised form, October 14, 1996)

Bing Kuang and Peter A. Rubenstein‡

From the Department of Biochemistry, College of Medicine, University of Iowa, Iowa City, Iowa 52242

Holmes proposed that in F-actin, hydrophobic residues in a subdomain 3/4 loop interact with a hydrophobic pocket on the opposing strand resulting in helix stabilization. We have determined how a decreased hydrophobicity of this plug affects yeast actin function. Cells harboring only the V266G, V266D, V266F, L267G, L269D, or L269K actins appear normal, although V266G cells display an altered budding pattern. However, V266G,L267G (GG) double mutant cells are cold-sensitive with randomly oriented thick actin assemblies seen in rhodamine phalloidin-stained GG cells. V266D actin polymerizes slower than wild-type actin at room temperature. At 4 °C, not only is polymerization slowed, but there is also an effect on critical concentration. However, the polymerization defects are milder than those associated with substitution of Asp for the neighboring Leu^{267}. Purified GG-actin does not polymerize *in vitro* alone or in the presence of wild-type F-actin seeds. GG-actin polymerization can be restored by larger amounts of wild-type actin, beryllium fluoride, or phalloidin at room temperature, although at 4 °C only phalloidin is effective. These results suggest that the diminished hydrophobicity of the plug in GG-actin leads to filament destabilization. However, the V266D actin results require a modification of the original Holmes filament model.

F-actin, a two-stranded helical polymer composed of actin monomers (G-actin), is involved in numerous cellular processes. Although the structure of G-actin has been solved to atomic resolution (1–3), the atomic structure of F-actin remains unresolved due to the inability to obtain F-actin crystals. Based on the atomic structure of rabbit skeletal muscle G-α-actin (1) and the x-ray fiber diffraction patterns of axially oriented F-actin gels, Holmes *et al.* (4) proposed an atomic model for the F-actin filament. Use of a directed mutation algorithm has produced a refined model with a high level of agreement between the diffraction pattern predicted from the model based on the monomer structure with that obtained from the fibers (5). This model agrees well with the structural model derived from other data fitting techniques (6, 7) and optical reconstruction of electron micrographs of actin filaments (8–10). The orientation of the monomer in the helix in this model agrees with the results of a genetic study of the F-actin binding site of phalloidin (11), chemical cross-linking experiments (12), and antibody decoration experiments (13, 14). However, there is little evidence concerning the validity of the model pertaining to the intermonomer contacts that stabilize the helix.

A central feature of this model is a postulated interaction of a hydrophobic plug at the tip of a loop between subdomains 3 and 4 with a hydrophobic pocket formed by the interface of two subunits on the opposing strand of the helix. Although the proposed interaction would constitute a major interstrand stabilizing force for the actin helix (Fig. 1*A*), there is no direct evidence in support of this plug-pocket interaction. In all three published structures of G-actin, the loop is parked against the surface of the actin monomer so that it would be incapable of interacting with the pocket on the opposing strand. Furthermore, there is no direct evidence that this loop rotates through the required 90° in any of the published structural studies of the filament. Finally, normal mode analysis of F-actin (7) does not predict the participation of this subdomain 3/4 loop in a rigid plug-pocket interaction as originally predicted by Holmes.

This model has been challenged by Schutt and colleagues (15) on the basis of the relatively low resolution of the electron microscopy measurements used to generate the Holmes model as well as problems with spacing of residues within the filament and the energetics needed for the conformation changes required by the model. They have proposed an alternative model for the actin filament based on the actin-actin contacts found in the actin-profilin ribbon structure that forms during crystallization of the profilin-β actin complex (2, 16). However, coordinates for this model have not been published, and it has therefore been difficult to analyze the results of experiments pertaining to actin filament structure in terms of the predictions of this model.

In *Saccharomyces cerevisiae* actin (Fig. 1*B*), which is 87% homologous with skeletal muscle actin, the plug residues F-I-G-M are replaced by Val^{266}-Leu^{267}-Gly^{268}-Leu^{269},[1] although the residues comprising the strands of the loop are almost identical between the two actins. As an initial test of the plug-pocket interaction model, we previously replaced Leu^{267} with aspartic acid (17), reasoning that if the plug-pocket interaction was important to filament integrity, such a substitution should destabilize the filament. Although this substitution produced only minimal effects *in vivo*, it resulted in a marked cold-sensitive polymerization defect *in vitro*. The rate of polymerization of pure mutant actin was retarded at room temperature, but the Cc[2] was only minimally affected. However, 19 μM

* This work was supported by National Institutes of Health Grant GM33689 (to P. A. R.). The costs of publication of this article were defrayed in part by the payment of page charges. This article must therefore be hereby marked "*advertisement*" in accordance with 18 U.S.C. Section 1734 solely to indicate this fact.

‡ To whom correspondence should be addressed: Dept. of Biochemistry, College of Medicine, 4403 Bowen Science Bldg., Iowa City, IA 52242-1109. Tel.: 319-335-7911; Fax: 319-335-9570.

[1] The L267D mutation was originally noted as L266D (17) to reflect the fact that we called the initiator Met residue of actin Met-1. However, since the initiator Met is retained in yeast actin, we have renumbered this residue.

[2] The abbreviations used are: Cc, critical concentration; DAPI, 4′,6′-diamidino-2-phenylindole; FM 4–64, *N*-(3-triethylammoniumpropyl)-4-(*p*-diethylaminophenylhexatrienyl) pyridinium dibromide; BeF_x, beryllium fluoride; WT, wild type.

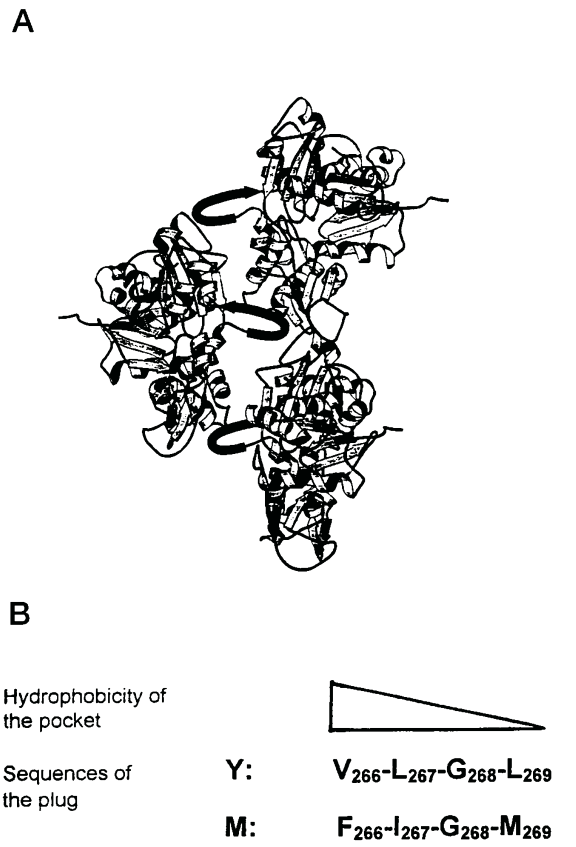

FIG. 1. **Molecular model for the orientation of three actin subunits in the rabbit skeletal muscle actin filament (*A*) (5).** The loop containing the hydrophobic plug is the dark element perpendicular to the filament axis. The DNase I binding loop is at the bottom of each monomer. *B,* the sequences of the hydrophobic plug in rabbit skeletal muscle actin (*M*) and yeast actin (*Y*) and the postulated hydrophobic strength of the plug-pocket interaction across the plug.

mutant actin could not polymerize at 4 °C. This defect could be rescued by the inclusion of phalloidin as a filament stabilizing agent.

These *in vitro* results were consistent with the Holmes model on two accounts. First, hydrophobic interactions are cold-sensitive (18), and the introduction of an acidic residue into this plug may have lowered its hydrophobicity to such a degree that at 4 °C, the residual hydrophobicity of the plug was not sufficient for helix stabilization. Second, rescue of polymerization by phalloidin showed that integrity of the monomer was not compromised by the mutation and that the major effect of the mutation was on the interstrand stabilization of the helix. On the other hand, besides the fact that normal mode analysis of F-actin does not predict the occurrence of a rigid plug-pocket structure, nothing is known about the relative contribution of the individual hydrophobic residues of the plug to actin stability or to what extent hydrophobicity of the plug can be lowered before significant disruption of actin function is observed. In essence, the central tenets of the plug-pocket model have yet to be verified.

The Holmes plug-pocket model leads to a number of predictions. First, the strongest hydrophobic contacts should involve the N terminus of the plug and the strength of the interaction should decrease toward the plug's C terminus (Fig. 1*B*). For example, with the muscle actin structure, the phenyl group of Phe^{266} is the part of the plug most deeply buried in the hydrophobic pocket. Second, at any position in the plug, substitution of a charged residue should produce a more drastic effect than simply eliminating the hydrophobic side chain of the residue normally at that position. Third, plug mutations that affect actin stability should be cold-sensitive. Finally, this model, coupled with our initial results, suggests there may be a "threshold effect" governing this interaction. Removal of one hydrophobic residue might not alter the hydrophobicity of the plug sufficiently to destabilize the helix. However, removal of multiple hydrophobic side chains or insertion of a charged residue should, at some point, disrupt the interaction of the plug with the pocket enough to lead to filament destabilization.

In this paper, using a yeast expression system, we have mutagenized each of the three hydrophobic plug residues to test the positional effects predicted by the Holmes model and to determine how hydrophobic the plug has to be for actin polymerization to occur. We replaced Val^{266} with Asp and Leu^{269} with Asp and Lys to compare the effects of a charged residue at both ends of the plug relative to those caused by a charge at residue 267. Second, we examined the effects of increasing the hydrophobicity of the first position to that of muscle actin (V266F) and of decreasing the hydrophobicity at positions 266 and 267 by making single substitutions of Gly for either Val^{266} or Leu^{267}. Finally, we converted both of these residues simultaneously to Gly creating a plug consisting of G-G-G-L in which most of the hydrophobicity of the plug was removed. We then assessed the extent of the defects caused by the mutations *in vivo* and *in vitro* and determined the efficacy of different approaches *in vitro* for overcoming the polymerization defects caused by the most severe of these mutations.

MATERIALS AND METHODS

Reagents—The Sculptor site-directed mutagenesis kit was purchased from Amersham Corp. Deoxyadenosine-5′-(α-thiotriphosphate, ^{35}S (1000–1500 Ci/mmol), was purchased from DuPont NEN. Phalloidin, DAPI, and fluorescent brightener 28 (Calcofluor) were purchased from Sigma. Rhodamine-phalloidin and FM 4–64 (*N*-(3-triethylammoniumpropyl)-4-(*p*-diethylaminophenylhexatrienyl) pyridinium dibromide) was from Molecular Probes (Eugene, OR). Pancreatic DNase I was obtained from Boehringer Mannheim. The Sequenase version 2.0 DNA sequencing kit was purchased from U. S. Biochemical Corp. Affi-Gel 10 active ester agarose was obtained from Bio-Rad. DE52 DEAE-cellulose was obtained from Whatman. Sephacryl S-200 resin was purchased from Pharmacia Biotech Inc. The BCA assay reagent was purchased from Pierce. The oligodeoxynucleotides used for site-directed mutagenesis were synthesized in the DNA Core Facility at the University of Iowa (Iowa City, IA).

Oligodeoxynucleotide-directed Mutagenesis and Plasmid Construction—As a template for the mutagenesis reactions, we used single strand DNA generated from the plasmid pGEM 3Z(−) into which the yeast actin gene and its promoter had been introduced between the *Bam*HI and *Eco*RI sites (19). The following oligodeoxynucleotides were used to generate the mutants we analyzed (in each case the mutant codon is underlined): 5′-CCATCCTTCTGGTTTGGGTTTGG-3′, V266G (VG); 5′-CCTTCTGTTTTGGGTAAGGAATCTGCCGGTATTG-3′, L269K;5′-CCTTCTGTTTTGGGTGATGAATCTGCCGGTATTG-3′, L269D; 5′-CCATCCTTCTG(G/T)TGGTGGTTTGGAATCTGCC-3′, L267G (LG) or the double mutant (GG) V266G,L267G; 5′-CCATCCTTCTTTTTTTGGGTTTGG-3′ V266F (VF); and 5′-CCATCCTTCTGATTTGGGTTTGG-3′ V266D.

The mutations were verified by sequencing, and all but one of the *Bam*HI-*Eco*RI fragments were subcloned into the centromeric yeast shuttle vector pRS314, which is marked by the *TRP1* gene (20). The coding sequence for V266D actin was cloned into a derivative of the centromeric yeast expression vector YCp50 marked with the URA 3 gene *pCENV266D.* (21).

Construction of Haploid Yeast Strains Expressing the Mutant Actins Only—We transformed the diploid yeast strain TDyDD (21), a gift of D. Shortle (The Johns Hopkins University, Baltimore, MD), with plasmids carrying the mutant actin sequences. This trp 1, ura 3–52 strain has one active chromosomal actin gene and one disrupted with the *LEU2* gene. Following transformation and sporulation, haploid colonies with the phenotype TRP/LEU were successfully identified for each mutant at a frequency comparable to that obtained when a WT actin sequence was used in the transforming plasmid. Cells carrying the V266D plasmid were selected in a different fashion. We began with a haploid derivative

of TDyDD that carried a chromosomal actin gene interrupted with the *LEU2* gene. Actin synthesis in this cell is driven by a wild-type actin gene contained in pRS314 as above. The cells were transformed with pCENV266D, and cells were ultimately selected for their ability to grow on uracil-deficient but not tryptophan-deficient medium. The plasmids were rescued from each of these strains according to Robzyk *et al.* (22), and the entire coding region sequenced to insure that the mutant sequences were intact. Two wild-type actin strains were prepared: one TDyDDWN-pCEN contained the wild-type actin coding sequence in the YCp50-derived plasmid, and TDyDDWN-PRS contained the wild-type coding sequence on the pRS-314-derived plasmid. The strains with mutant actins were named according to the mutant actins they carried: TDyV266G, TDyV266F, TDyV266D, TDyL267G, TDyL269D, TDyL269K, and TDyGG, the double mutant. Cells were grown either in liquid YPD (2% Bacto-peptone, 1% yeast extract, and 2% glucose), on solid YPD medium (liquid YPD medium containing 2% agar), or in liquid or solid defined medium (23).

Fluorescence Microscopy—Yeast haploid cells were grown to an OD_{600} of about 0.5–0.8 and processed as follows. Chitin deposition was visualized by staining with Calcofluor (24). Yeast actin cytoskeletons were visualized by staining with rhodamine phalloidin (25). Nuclei were stained with DAPI (26). Vacuoles were visualized according to Vida and Emr (27). Here, log phase cells were labeled with the styryl dye FM 4–64 at 30 °C for 1 h and then chased for 3 h with added fresh YPD media at 30 °C. Cells were then collected for observation. Fluorescence micrographs were obtained on a Carl Zeiss microscope (Oberkochen, Germany) using Kodak T-MAX 400 film (Eastman Kodak Co.). To assess the percentage of cells with defective phenotypes, we always scored more than 100 cells by microscopy.

Examination of Growth Characteristics of the Mutant Yeast Strains—To assess the ability of the cells to grow in hyperosmolar medium or in glycerol containing medium, the cells were grown on YPD plates for one day. The cells were then replica-plated to YPD plates, hyperosmolar plates (YPD containing 0.9 M NaCl), or YPG plates (2% glycerol instead of glucose). Plates were photographed at different times during the incubations. For the TDyV266D cells, an isogenic wild-type strain TDyDDWN-pCEN was used as a control. For the other mutant cells, the control was the isogenic wild-type strain TDyDDWN-PRS. The two wild-type strains had identical growth rates at 30 °C, but strain TDyDDWN-PRS grew about 40% faster at 10 °C than did TDyDDWN-pCEN.

The generation times for each strain in liquid YPD at different temperatures were determined as follows. Following growth overnight in YPD, cells were diluted into 10 ml of fresh YPD preincubated at the desired temperature, and the cultures were incubated at the desired temperature in a rolling drum apparatus. Aliquots were removed at desired intervals and the cell density at 600 nm was measured. Triplicates of each strain were followed, and the growth of wild type and mutant cells was assessed at the same time. The ranges for the determination were less than 5% of the mean.

Actin Purification—Mutant actins were purified from the appropriate cells using the DNase I-agarose procedure of Cook *et al.* (21) in the Ca^{2+}-G form and stored at 4 °C in Ca^{2+}-G-buffer (10 mM Tris-HCl, pH 7.5, containing 0.2 mM $CaCl_2$, 0.2 mM ATP, and 0.5 mM dithiothreitol). Wild-type actin was purified from cakes of *S. carlsbergensis* obtained at a local bakery. The sequence of this actin is identical to that from *S. cerevisiae* (28). Actins were used within 4 days following completion of purification. Since the GG-actin was likely to be cold-sensitive, its polymerization during purification was carried out at room temperature. Following centrifugation, a clear gelatinous pellet was observed as was the case for the other mutant actins, although the GG-actin solution was decidedly less viscous than the other actins prior to centrifugation. We obtained about 2–3 mg of actin from 10 liters of cell culture in which the cells were grown to stationary phase. However, because of the difficulty in inducing GG-actin monomers to self-associate, it was important to concentrate the unpolymerized actin to a smaller volume than used with the other mutant actins prior to induction of association by the addition of salt to avoid losing a large percentage of the protein in the supernatant fraction following centrifugation. Where noted, the actin was further purified by passage over Sephacryl S-200 equilibrated in Ca^{2+}-G-buffer to eliminate residual actin oligomers. Protein concentrations were determined by the Pierce BCA assay using bovine serum albumin as a standard. All actins were purified to a single band as determined by electrophoresis in SDS on 10% polyacrylamide gels. Ca^{2+}-G actins were converted to the Mg^{2+} forms according to Strzelecka-Golaszewska *et al.* (29).

Actin Polymerization—Actin polymerization assay and critical concentration determination were done according to Chen *et al.* (17). In experiments that examined the ability of BeF_x to stabilize mutant F-actin, 5 mM NaF and 0.1 mM $BeCl_2$ were added to the samples of G-actin just prior to induction of polymerization (30).

For visualization of actin filaments, samples were polymerized at the desired temperature for 1 h, and samples were then deposited on carbon-coated Formvar grids. The grid was washed and stained with 1.5% uranyl acetate. The samples were then examined with a model 7000 electron microscope (Hitachi Instruments Inc., San Jose, CA) in the University of Iowa Central Electron Microscope Facility.

TABLE I
Doubling times for WT and GG haploid cells at different temperatures

Cells	Temperature (°C)				
	10	15	23	30	37
			h		
WT	22.8	8.4	3.3	2.1	2.6
GG	Growth arrest	30.5	6.1	3.5	6.6

RESULTS

Growth Characteristics of Strains with Mutant Actins—Because hydrophobic interactions tend to weaken as the temperature decreases, Holmes' model suggests that any growth defect due to diminished hydrophobicity of the hydrophobic plug should be more pronounced as the growth temperature is lowered. We thus determined the growth rates of wild-type cells and cells expressing each of the mutant actins. TDyV266D cells grow normally at 30 °C but exhibit about a 25% decreased rate of growth at 10 °C in comparison to wild-type cells, similar to what we previously observed when the negative charge was placed at Leu^{267}. Cells containing the other actins with single mutations display little or no difference in generation time at temperatures between 10 °C and 37 °C when grown in liquid YPD.

At 30 °C, the optimal growth temperature for yeast, GG cells grew at roughly 40% of the rate of wild-type cells (Table I). Decreasing the growth temperature caused an increase in the generation time of the GG cells relative to the wild-type cells such that after 50 h at 10 °C, growth of the GG cells arrested. This cold sensitivity was much more severe than that noted with the V266D cells or previously with the L267D (17). Increasing the temperature to 37 °C also produced a significant decrease in the growth rate of GG compared with wild-type cells, suggesting they were somewhat temperature-sensitive. Use of a plating assay to measure growth of GG cells at 15 and 30 °C produced the same results.

Exposure of yeast to hyperosmolar conditions causes a restructuring of the actin cytoskeleton (31), and some actin mutations have been shown to result in osmosensitive cells (31, 32). Of the mutant cells studied here, only the GG cells showed retarded growth on hyperosmolar plates (Fig. 2). After 2–3 days' incubation at 30 °C, growth of the GG cells was virtually nonexistent, although the cells seemed to recover over the next 2–3 days. These results may reflect the inability of the GG-actin to properly nucleate filament formation or form stable filament assemblies in response to the environmental stress. All of the mutant strains appeared to grow normally on plates containing 2% glycerol as a sole carbon source, although we did not determine the generation times of the cells in liquid medium containing glycerol.

Morphology of GG Cells—In yeast, actin is an important determinant of cell polarity and cell size and shape (11, 32). Microscopic examination of V266G, V266D, V266F, L267G, L269K, and L269D cells showed that their size and morphology is normal. However, the diameter of GG cells is generally larger than that of wild-type cells, and 10% of the GG cells are about 3 times larger in diameter than that of wild-type cells (Figs. 3*E,* 4*C,* and 5*C*). Staining with Calcofluor showed that V266F, V266D, L267G, L269K, and L269D cells displayed well-formed

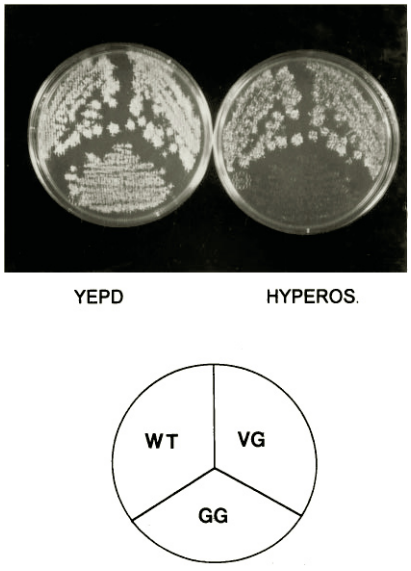

FIG. 2. **The GG mutation retards the growth of haploid cells on hyperosmolar medium.** TDyWT-PRS, TDyV266G, and TDyGG haploid cells were streaked on a YPD plate and incubated at 30 °C. The plate was replica-plated on YPD/0.9 M NaCl and YPD plates which were incubated at 30 °C. The photograph was taken after 50 h. After another 50 h, a lawn of GG cells is evident on the hyperosmolar plate (data not shown).

chitin rings at the sites of previous budding events and the axial budding polarity typical of yeast. Although chitin was also localized in V266G cells, these cells displayed a random budding phenotype approximately 30% of the time (Fig. 3*D*), indicating that the V266G mutation caused a mild abnormal phenotype *in vivo* not observed with the L267G or the more drastic V266D mutation. For the GG cells, the chitin was delocalized in 86% of the 100 cells observed (Fig. 3*F*), suggesting the presence of a significant secretion defect resulting from elimination of the hydrophobic side chains of Val^{266} and Leu^{267}.

In yeast, actin plays a role in mitotic spindle orientation and migration (33), and yeast morphogenetic mutants usually are defective in nuclear segregation (11, 34). The large size of GG cells and the cell polarity defect suggests that the GG mutation may have significantly compromised proper nuclear segregation. We thus examined cells stained with DNA directed dye DAPI. About 12% of the GG cells contain either two or more nuclei (Fig. 4).

Actin has been implicated in vacuolar morphology determination and vacuolar segregation (35)[3] in *S. cerevisiae*. We investigated vacuolar morphology and localization in TDyGG cells using a vacuole membrane specific dye FM 4–64 (27). In around 40% of the GG cells, the vacuole appears either as a large single lobe or as one with a few large lobes instead of a collection of small multilobed bodies typical of wild-type cells (Fig. 5). Five percent of these cells also show a defect in vacuolar segregation. These results suggest that the GG mutation produces an abnormal topology and/or distribution of actin filaments leading to the altered vacuole and nuclear segregation behavior we observe.

The Actin Cytoskeleton of GG Cells—To visualize the actin cytoskeleton directly, we stained wild-type and mutant cells with rhodamine-phalloidin. The cytoskeletons of V266G, L267G, L269K, and L269D cells appeared normal with actin cables in the mother cells along the growth axis of the cell and actin patches primarily in the buds in the early stages of the cell cycle. However, GG cells contain a markedly altered cytoskeleton with cables generally absent in the mother cell and bright patches in both the mother cell and bud (Fig. 6). At 30 °C, randomly oriented thick actin bars or ribbons are present in approximately 10% of the cells. Growth at 10 °C for 16 h produces these abnormal assemblies in roughly 30% of the cells observed (Fig. 6*C*). This abnormal cytoskeletal structure is consistent with the aberrant growth and morphology associated with these cells and again suggests that the GG mutation

[3] K. Hill and L. Weisman, personal communication.

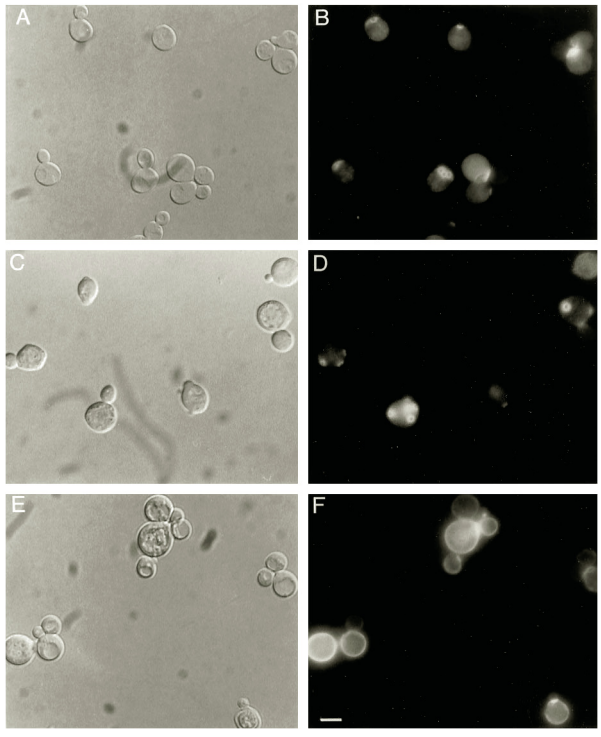

FIG. 3. **Calcofluor staining of cells containing V266G and GG mutant actins.** Log phase haploid cells grown at 30 °C were stained with Calcofluor. *A, C,* and *E* show differential interference contrast images of WT, V265G, and GG cells, respectively. *B, D,* and *F* show the Calcofluor staining patterns of these cells. *Scale bar,* 5 μm.

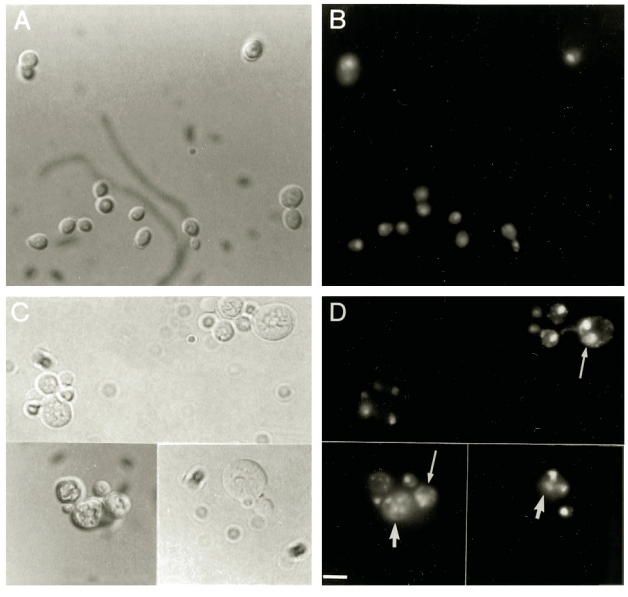

FIG. 4. **Nuclear segregation defect in GG mutant cells.** Log phase haploid cells grown at 30 °C were stained with DAPI. *A* and *C* are differential interference contrast images of WT and GG cells. *B* and *D* show the DAPI staining patterns of these cells. In *D,* the *thick arrows* point to multinucleated cells, and the *thin arrows* point to binucleated cells. *Scale bar,* 5 μm.

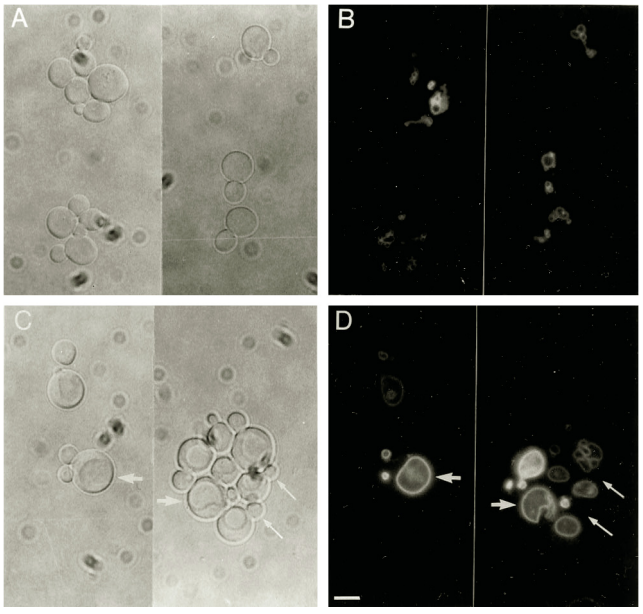

FIG. 5. **Altered vacuole morphology and segregation errors in cells with GG-actin.** Log phase haploid cells grown at 30 °C were stained with FM 4–64. *A* and *C* show differential interference contrast images of WT and GG cells. *B* and *D* show the corresponding FM 4–64 staining patterns. In *C* and *D,* the *thick arrows* point to cells with a single big vacuole and the *thin arrows* point to buds lacking a visible vacuole. *Scale bar,* 5 μm.

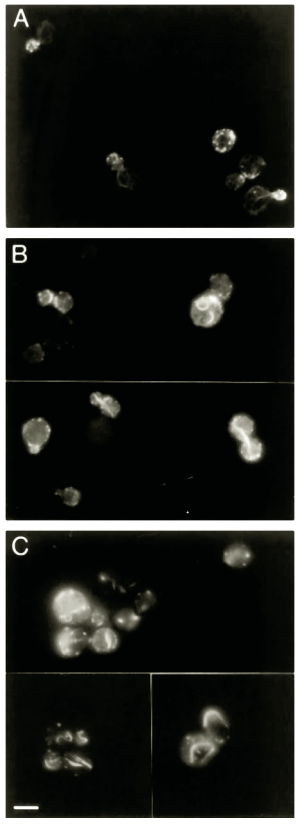

FIG. 6. **Actin cytoskeletal organization of cells containing GG-actin.** Log phase haploid cells grown at 30 °C were stained with rhodamine-phalloidin or incubated at 10 °C for 16 h and then stained with rhodamine-phalloidin. *A,* 30 °C WT; *B,* 30 °C GG; *C,* 10 °C GG. *Scale bar,* 5 μm.

causes a cold-sensitive defect in actin function. The disorganization of actin structures in the GG cells implies either a defect in actin polymerization or the inability of GG-actin to interact properly with various actin binding proteins *in vivo*.

Polymerization Defects of V266D and GG-actins in Vitro—To begin to assess the molecular basis of the defect associated with the GG mutation, we assessed the polymerization characteristics of the different purified mutant actins. Our ability to obtain these mutant actins by our normal purification protocol indicates that the different mutations have no major deleterious effect on the integrity of the actin monomer. Gel-filtered V266G, V266F, L267G, L269K, and L269D actins in the Ca^{2+} form polymerized normally in comparison with WT actin at temperatures between 4 and 25 °C (data not shown). Furthermore, negatively stained samples of filaments made from these actins appeared normal by electron microscopy. Thus, abolition of hydrophobicity from either of the first two residues of the plug or introduction of a charged residue in the last position did not affect the interactions governing actin polymerization. The results with the Leu^{269} substitution are markedly different than the disruption of polymerization caused by introduction of a charged residue at position 267 (17).

Although substitution of a charged residue at position 269 produced no apparent polymerization defect, substitution of Asp for Val at position 266, the N-terminal end of the plug, produced a noticeable defect. At 25 °C, the extent of polymerization of V266D actin was essentially the same as WT actin, although its rate of polymerization was slightly but reproducibly retarded (Fig. 7*A*). In comparison, at room temperature we previously showed that while there was little change between the Cc of WT and L267D actin, the difference in the rates of polymerization of the L267D and WT actins was much greater than with the V266D actin. At 4 °C, the difference in polymerization rates was much more pronounced with apparent adverse effects of temperature on both the nucleation and elongation phases of the process, although we did not study the elongation phase separately (Fig. 7*B*). Significantly, however, the extent of polymerization of V266D actin was almost the same as wild-type actin. We next determined the extent to which cold temperature adversely affected the critical concentration of V266D actin. Using two different preparations of wild type and mutant actin, we found that the critical concentrations of the two actins were essentially the same (0.35–0.45 μM). However, at 4 °C, the Cc for WT and V266D actins were 0.94 and 1.7 μM for one experiment and 1.1 and 2.1 μM, respectively, for a second set. Thus, as with L267D actin, V266D actin also showed a definite temperature effect on Cc. However, the extent of the effect was much less than observed with L267D actin, which failed to polymerize at 20 μM and gave a critical concentration of 11 μM when F-actin formed at room temperature was diluted into cold F-buffer (17).

Of the mutants we assessed, the GG mutation most drastically affected actin polymerizability in agreement with the relative effects caused by this mutation *in vivo*. Ca^{2+}-GG-actin at a concentration of 19 μM showed no evidence of polymerization at 25 °C, whereas at 25 °C polymerization of the other two cold-sensitive mutant actins, L267D (17) and V266D, were only somewhat retarded. Even at 70 μM, GG-actin forms only small amorphous aggregates barely detectable by light scattering (Fig. 8*B*). This cold sensitivity is compatible with the participation of the hydrophobic plug in a hydrophobic interaction that either leads to cross-strand stabilization or maintenance of monomer structural integrity.

If the major defect of GG-actin is its inability to form stable nuclei which can then be elongated, introduction of phalloidin-stabilized WT actin seeds to GG-actin might rescue polymerization. However, no polymerization was seen following addition of 0.05 μM actin seeds to 19 μM Ca^{2+}-GG-actin at 25 °C. We then added increasing amounts of WT actin to the GG-actin to determine whether the normal actin could provide enough

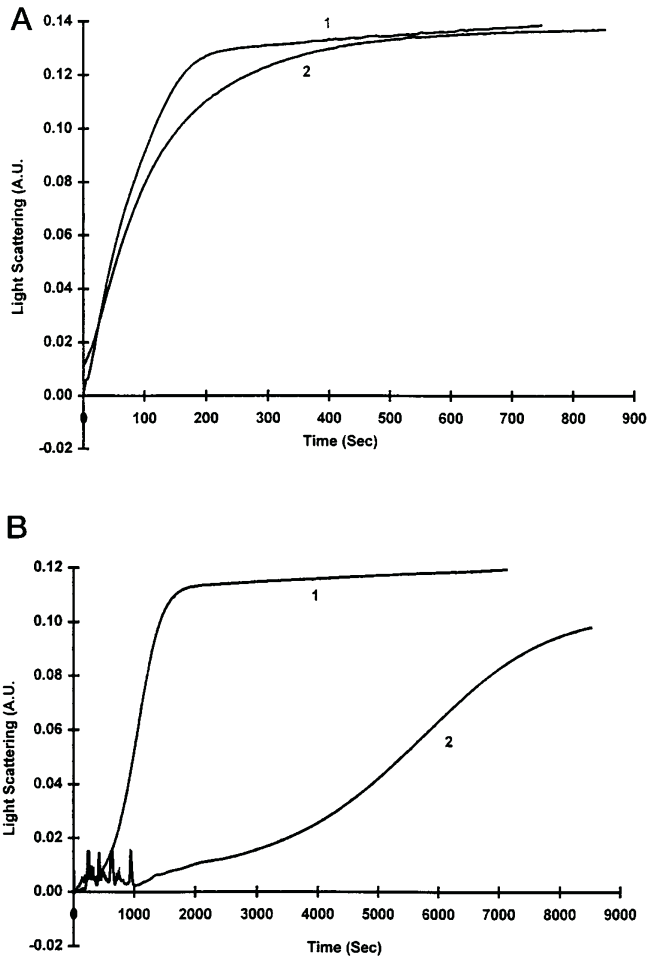

FIG. 7. **Polymerization of Ca^{2+}-wild type and V266D actins at room temperature and 4 °C.** Polymerization of the Ca^{2+} forms of the actins were followed as a function of time using a light-scattering assay. All actin concentrations were 7 μM. *A,* polymerization at room temperature; *B,* polymerization at 4 °C.

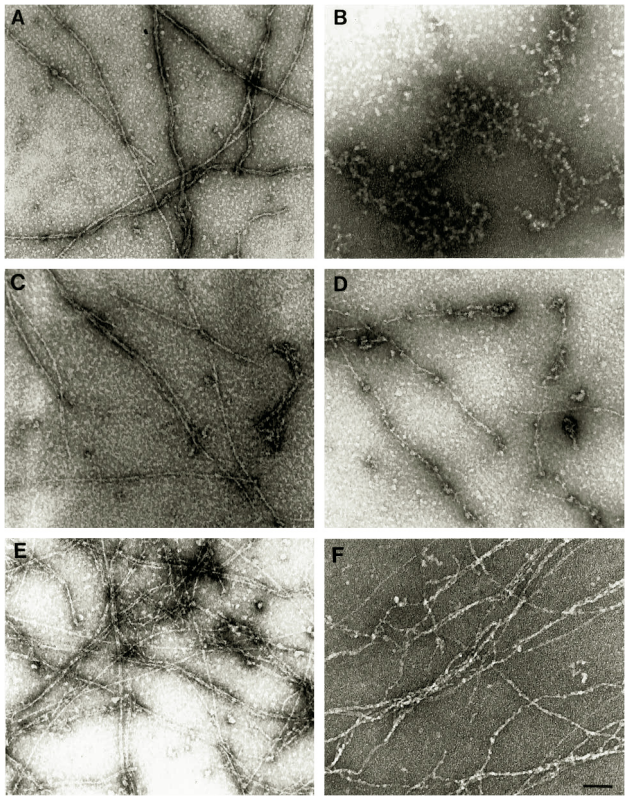

FIG. 8. **Electron micrographs of uranyl acetate-stained filaments formed by GG-actin in the presence of wild-type actin, BeF_x, or phalloidin.** Ca^{2+}-actins were polymerized at 25 °C for 1 h except for panel *F,* in which the sample was polymerized for 2 h at 4 °C. *A,* 5 μM WT; *B,* 70 μM GG; *C,* 2.4 μM WT plus 16.6 μM GG (1:7 ratio); *D,* 1.2 μM WT plus 17.8 μM GG (1:15 ratio); *E,* 19 μM GG plus BeF_x; *F,* 19 μM GG plus equimolar phalloidin at 4 °C. *Scale bar,* 0.1 μm.

cross-strand helical stabilization for the mutant actin to polymerize. Fig. 9*A* shows that at 25 °C, 90% of the total actin in a 19 μM actin solution containing 50% WT and 50% GG-actin polymerized. As the percent of WT actin in the mixture decreased, the total actin that polymerized also decreased such that a WT/GG ratio of 1:7 allowed only about 50% of the total actin to polymerize.

An increase in light scattering is consistent with aggregation as well as filament formation. We thus examined samples of the WT/GG-actin mixtures by electron microscopy. Fig. 8*C* shows that normal filaments were observed in the WT/GG mixture at a ratio of 1:7. Even at a ratio of 1:15, filaments were seen, although they appeared much shorter and more irregular than in the other samples (Fig. 8*D*). We then repeated the kinetics experiments at lower temperatures. As the temperature drops, the degree of actin polymerization for the mixture also decreases until at 4 °C, we observed almost no increase in light scattering above that which would be expected for the wild-type actin present in the mixture (Fig. 9, *B* and *C*).

Although these experiments were carried out with Ca^{2+}-actin *in vivo*, the high affinity cation binding site is probably occupied by Mg^{2+} (36). Since Mg^{2+}-actin also hydrolyzes ATP faster and polymerizes faster than does Ca^{2+}-actin (37, 38), we tested whether substitution of Mg^{2+} for Ca^{2+} in GG-actin would enhance its ability to polymerize. At 20 °C, addition of salt to monomeric Mg^{2+}-GG-actin causes an initial association of monomers (Fig. 10*A*). However, the light scattering soon disappears, and no actin filaments can be observed in this solution by electron microscopy. Mixtures of Mg^{2+} WT and GG-actins showed polymerization behavior similar to that observed with the Ca^{2+}-actins (Figs. 9 and 10). At 4 °C, addition of salt to a G-actin solution containing 2.4 μM wild-type and 16.6 μM Mg^{2+}-GG-actin caused an increase in light scattering, whereas none was observed for the Ca^{2+}-actins (Fig. 9*C, curve 6* and Fig. 10*C, curve 5*). Electron microscopy revealed actin filaments, and the degree of light scattering observed suggested that the filaments contained some GG-actin since no increase in light scattering occurred with just the 2.4 μM WT actin alone under these conditions. Thus, replacement of Ca^{2+} with Mg^{2+} rescued some ability of the GG-actin to polymerize, although the extent to which it polymerized was still extremely cold-sensitive.

Phalloidin is thought to stabilize actin filaments by forming connections between monomers both within and between strands of the helix (5, 11). To test whether phalloidin could restore the the ability of GG-actin to polymerize, we added 19 μM phalloidin to a mixture of 16.6 μM Ca^{2+}-GG-actin and 2.4 μM WT actin at 4 °C prior to the addition of salt. Polymerization occurred immediately and continued until essentially all of the actin in the sample had polymerized (data not shown). Phalloidin even allowed pure GG-actin to polymerize at 4 °C (Fig. 11). This increase in light scattering following addition of salt to GG-actin is not due to mere aggregation of the monomers as evidenced by the appearance of helical filamentous structures (Fig. 8*F*). Furthermore, these filaments produced a arrowhead pattern when stained with myosin S1 (data not shown). At this concentration, WT actin still polymerized markedly faster in the absence of phalloidin than did GG-actin

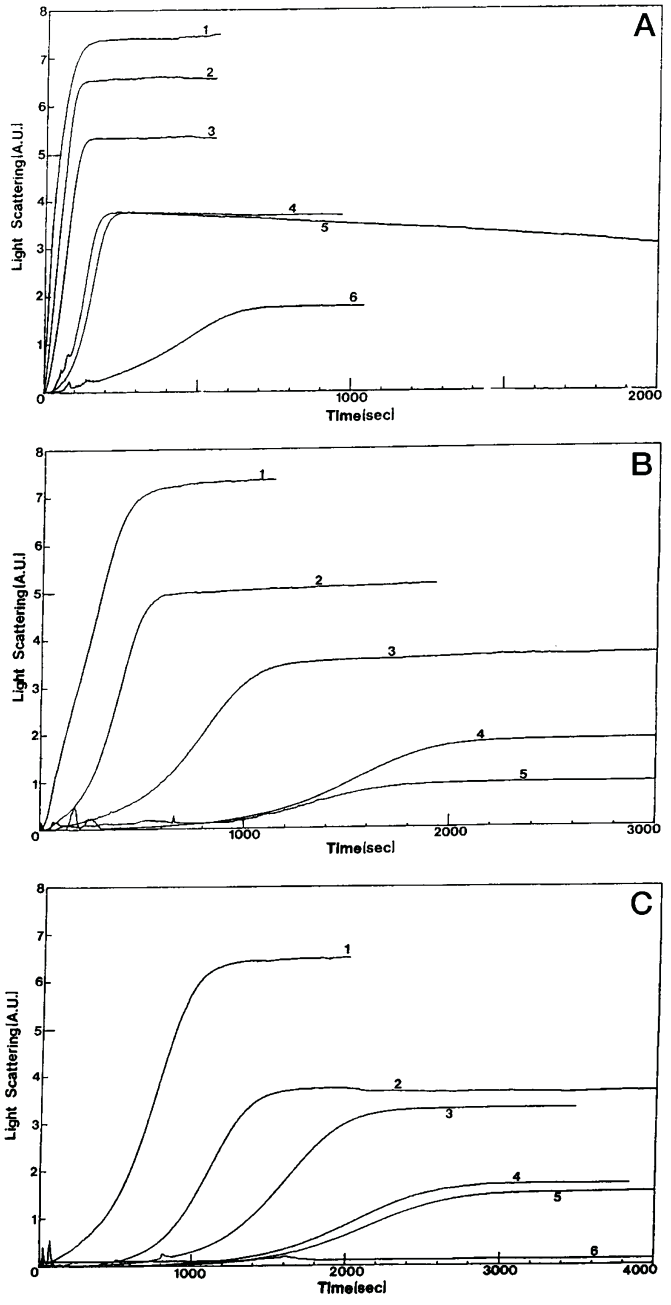

FIG. 9. **Polymerization of Ca^{2+}-wild-type and GG-actins at different temperatures.** Polymerization of Ca^{2+}-actin was followed as a function of time using a light-scattering assay. For the experiments with mixed actins, the total actin concentration was 19 μM and the WT/GG-actin ratios in the mixture are given. For WT controls, the concentrations of WT actin are given. *A,* 25 °C: *1,* 19 μM WT; *2,* 1:1; *3,* 1:2; *4,* 1:7; *5,* 1:15; *6,* 5 μM WT. *B,* 10 °C: *1,* 19 μM WT; *2,* 1:1; *3,* 9.5 μM WT; *4,* 5 μM WT; *5,* 1:7. *C,* 4 °C: *1,* 19 μM WT; *2,* 1:1; *3,* 9.5 μM WT; *4,* 5 μM WT; *5,* 1:3; *6,* 1:7.

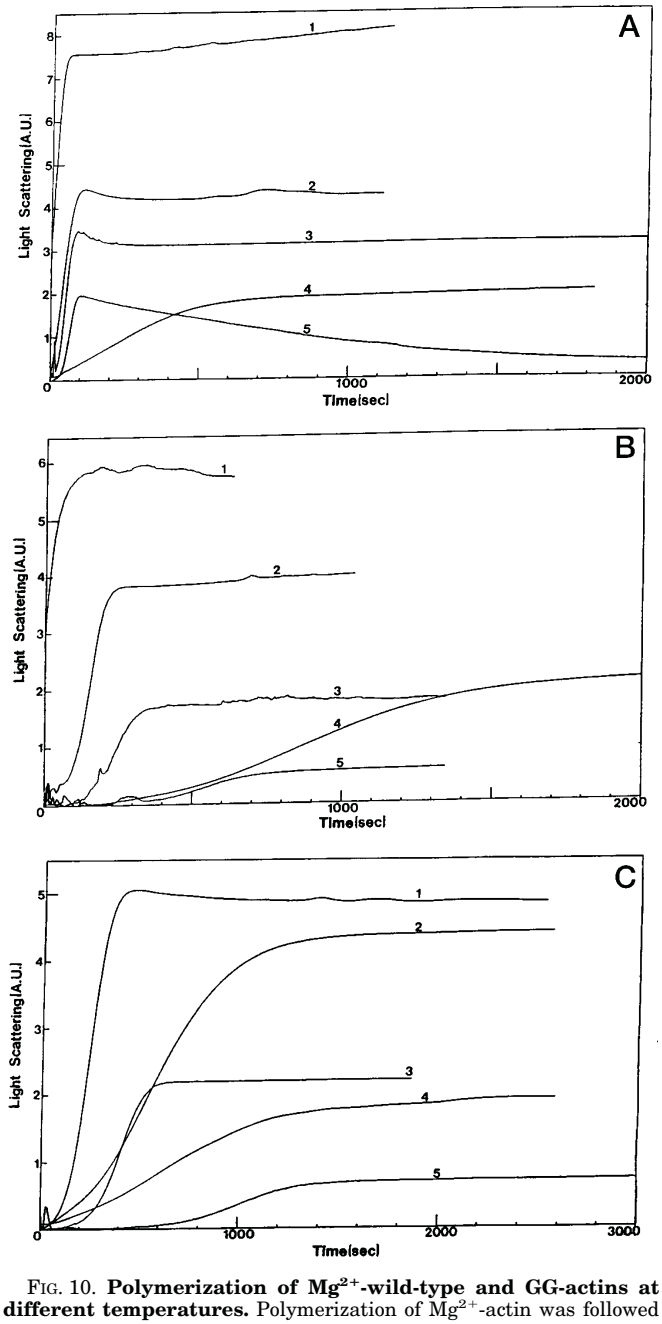

FIG. 10. **Polymerization of Mg^{2+}-wild-type and GG-actins at different temperatures.** Polymerization of Mg^{2+}-actin was followed as a function of time using a light-scattering assay. For the experiments with mixed actins, the total actin concentration was 19 μM, and the WT/GG-actin ratios in the mixture are given. Otherwise, the concentrations of actin are given. *A,* 20 °C: *1,* 1:1; *2,* 1:7; *3,* 1:15; *4,* 5 μM WT; *5,* 19 μM GG. *B,* 10 °C: *1,* 1:1; *2,* 1:3; *3,* 1:7; *4,* 5 μM WT; *5,* 1:15. *C,* 4 °C: *1,* 1:1; *2,* 9.5 μM WT; *3,* 1:3; *4,* 5 μM WT; *5,* 1:7.

in the presence of phalloidin (Fig. 8*C, curve 1*). The rescue of GG-actin polymerization by phalloidin further demonstrates that the GG mutation has no major deleterious effect on the integrity of the actin monomer under the conditions tested.

The previous experiments examined the ability of GG-actin to polymerize. We next determined the cold sensitivity of F-actin polymerized at 25 °C from a 19 μM Ca^{2+}-actin solution containing WT and GG-actins in a ratio of 1:7. Fig. 12 shows that each drop in temperature caused a corresponding decrease in the degree of polymerization. Furthermore, there was almost an immediate response between decreasing the temperature and the decrease in polymerization when the temperature was decreased at a rate of 1 °C/min (data not shown). At two points, when the temperature was held constant at a lower level, the degree of light scattering also remained constant over the period observed. At 4 °C, polymerization appeared to decrease to a level observed with 2.4 μM WT actin alone. When a 1:1 actin mixture was used, the same results were seen (data not shown). Our previous work (17) showed that such a decrease in temperature had little if any effect on the critical concentration of WT actin.

Effect of Nucleotide on the Stability of Filaments Containing GG-Actin—The nature of the nucleotide bound in the interior of the actin monomer affects the stability of the actin filament

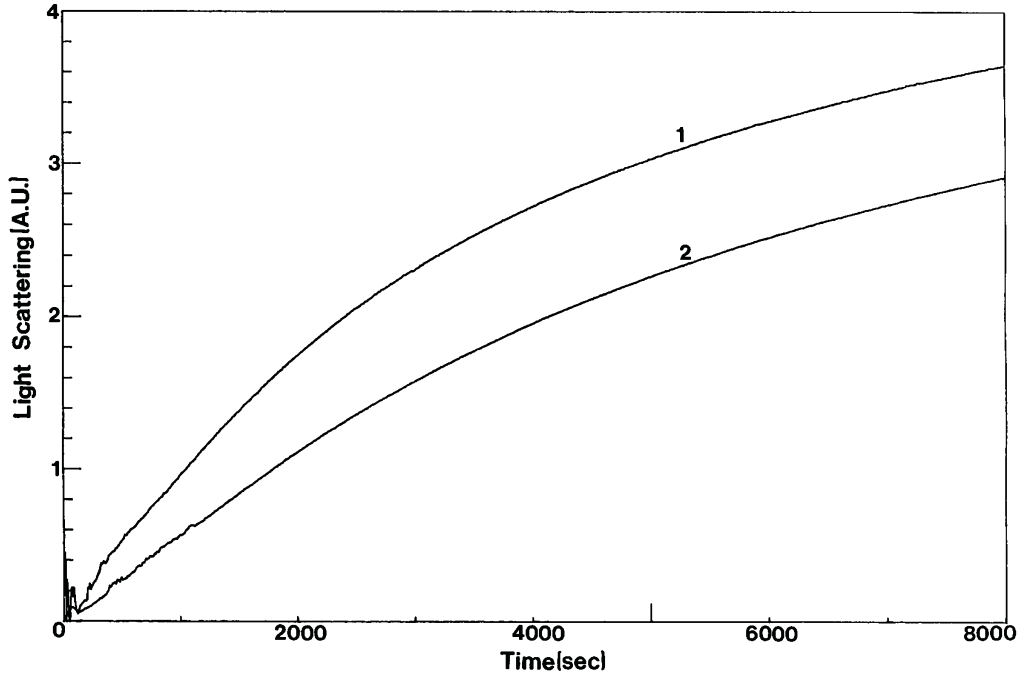

FIG. 11. **Phalloidin rescues the polymerization defect of GG-actin at 4 °C.** Polymerization of pure GG-actin in the presence of equimolar phalloidin at 4 °C was monitored by light-scattering assay. *1,* 19 μM Mg^{2+}-GG-actin; *2,* 19 μM Ca^{2+}-GG-actin.

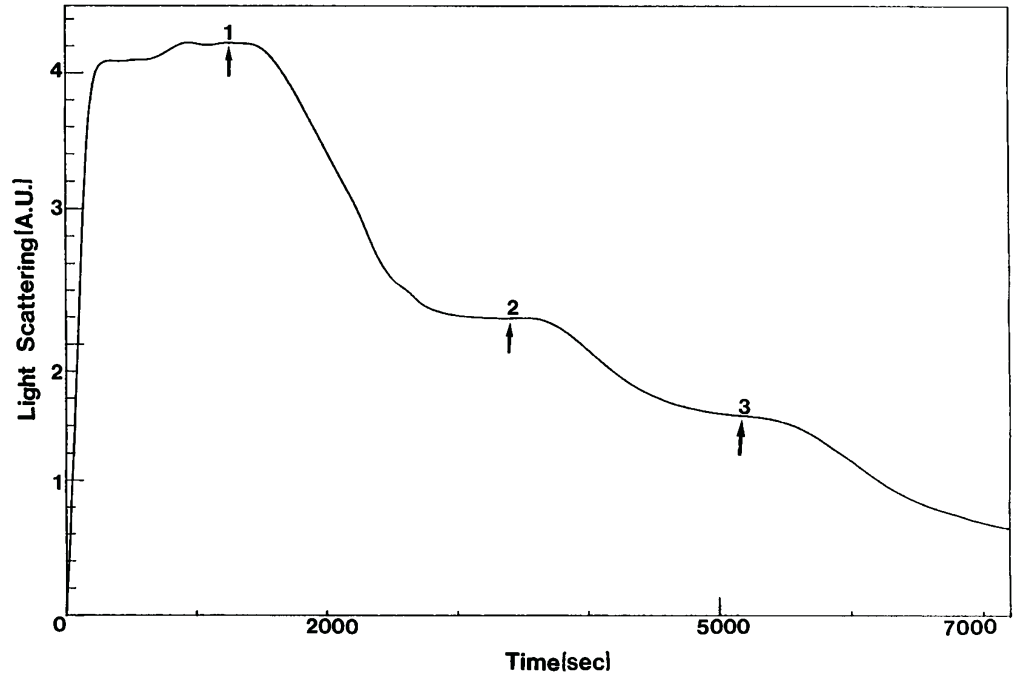

FIG. 12. **Temperature dependence of the stability of the preformed mixed wild-type and GG-actin filaments.** A mixture of 2.4 μM Ca^{2+}-WT and 16.6 μM Ca^{2+}-GG-actin was polymerized at 25 °C and then subjected to decreasing temperature. The extent of polymerization as a function of time was monitored by light scattering. *1*, time at which the temperature began to be lowered to 15 °C; *2*, time at which the temperature began to be lowered further to 10 °C; *3*, time at which the temperature began to be lowered to 4 °C.

(39, 40). After an actin monomer is incorporated into a filament, its ATP is hydrolyzed. The P_i that is generated is then slowly released producing a filament composed primarily of ADP actin which is less stable than one in which ATP hydrolysis and phosphate release has not occurred (41). At 25 °C, with a 19 μM Ca^{2+}-actin mixture containing WT and GG-actins in a ratio of 1:15, polymerization reached an initial plateau (Fig. 13, *curve 1*). After an extended period of time, this plateau decreased by about 30%. With mixtures containing higher percentages of WT actin, this decrease was less noticeable. Performance of the same experiment with Mg^{2+}-actin showed a decrease in polymerization as well but to a much smaller extent than that observed with Ca^{2+}-actin (Fig. 13, *curve 2*).

This decreased polymerization could reflect either an inherent inability of the GG-actin to maintain a stable filament structure or a filament instability due to a decreased ability of the GG-actin to bind to an actin filament composed largely of ADP-actin monomers. BeF_x binds tightly to F-actin and stabilizes the filament by acting as a phosphate analogue and occupying the P_i site vacated in the conversion of ATP- to ADP-actin (42). Based on the Holmes model, Orlova and Egelman (43) have suggested that the incorporation of BeF_x stabilizes the

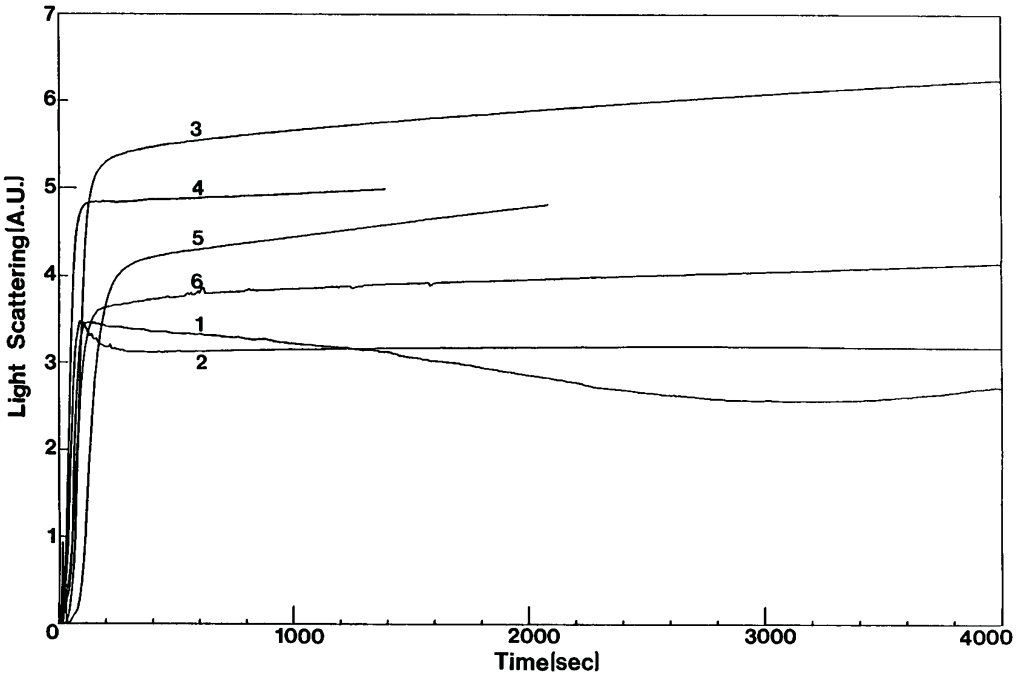

FIG. 13. **Effect of BeF_x on the polymerization of GG-actin.** Polymerization of GG-actin in the presence or absence of BeF_x was followed by light scattering. For all experiments, the total actin concentration was 19 μM, and the divalent cation form of the G-actin is shown. The ratios indicate the proportion of WT to mutant actin in each case. *1,* Ca^{2+}-(1:15), 25 °C; *2,* Mg^{2+}-(1:15), 20 °C; *3,* Ca^{2+}-(1:15), 25 °C with BeF_x; *4,* Mg^{2+}-(1:15), 20 °C with BeF_x; *5,* Ca^{2+}-pure GG, 25 °C with BeF_x; *6,* Mg^{2+}-pure GG, 20 °C with BeF_x.

helix by strengthening the contacts between subdomain 2 of one monomer with the monomer immediately above it in the filament. We thus repeated the polymerization of the 1:15 mixture in the presence of BeF_x. BeF_x not only prevents the polymerization decrease originally noted but increases the extent to which polymerization occurs (Fig. 13). With pure GG-actin, as was the case with phalloidin, the incorporation of BeF_x permitted polymerization of the pure mutant actin, and the increased light scattering observed in this experiment represents authentic filament formation (Fig. 8*E*). However, contrary to what we observed with phalloidin, BeF_x could not rescue polymerization of pure Ca^{2+} or Mg^{2+} GG-actin at 10 or 4 °C.

DISCUSSION

The effects associated with these "hydrophobic plug" mutations establish the importance of these residues in the formation and stabilization of F-actin. Although these effects generally correlate with those predicted by the Holmes model, our results were somewhat surprising based on the predictions of the original model. *In vivo*, the effects of these mutations are milder than what one might have predicted based on the central role proposed for this loop in actin helix stabilization. Substitution of a charged residue for leucine at the C-terminal end of the plug produced no observable abnormal phenotype whereas a similar substitution in either of the first two N-terminal plug residues produced a mild cold-sensitivity, suggesting the involvement of these residues in a necessary hydrophobic interaction. No such phenotype was seen when glycine was substituted at either of these positions. We did, however, see a budding polarity phenotype associated with the V266G but not with the V266D mutation. This budding phenotype is absent with the more severe aspartic acid substitution, and the mutation does not lead to cold sensitivity or other noticeable polymerization defect in the cells. Thus, it probably reflects a change in the conformation of the outside surface of the filament caused by the mutation rather than a destabilization. Finally, an apparent threshold effect is shown by the GG mutation in which the first two hydrophobic residues of the plug were replaced by glycines. In contrast with the phenotype associated with either single substitution, the effects *in vivo* of the double mutation caused a marked alteration in actin filament deposition within the cell along with other growth abnormalities.

In vitro, the effects of the mutations are more severe than those seen *in vivo*. As predicted, substitution of a charged residue at the N terminus of the plug was much more disruptive of polymerization than at the C terminus. Further, substitution of either of the N-terminal hydrophobic residues with an acidic amino acid markedly affected polymerization while substitution of single glycine residues did not.

However, in terms of the original model, two unexpected findings emerged from studying these mutations. First was the apparent absence of a polymerization defect caused by insertion of a charged residue for the C-terminal leucine. This result indicates that there must be considerable room in the filament to accommodate the charges of altered side chains in what had been proposed to be a hydrophobic region. Additionally, the leucine side chain usually at this position contributes marginally to stabilization of the helix when in the presence of the normal hydrophobic residues at positions 266 and 267. The second and even more unexpected observation was that substitution at the interior residue, Leu^{267}, produced a much more drastic effect on filament stability than substitution at the N-terminal residue Val^{266}. In the original filament model, Phe^{266} is the most deeply embedded in the hydrophobic pocket and is associated with the largest number of hydrophobic interactions. Since the pocket residues in the two actins are essentially the same, substitution for the valine should have been more disruptive than substitution for the neighboring leucine if the plug-pocket interaction was rigid.

The most striking result of this study is the behavior associated with the GG-actin *in vitro*. In this mutant actin, the only remaining hydrophobic residue of the plug is Leu^{269} which, under normal conditions, has little or no apparent importance

in actin helix stabilization. Results with this double mutation agree with the "hydrophobicity threshold" prediction derived from the Holmes model. In this context, removal of the side chain of any one hydrophobic residue does not alter the subunit-subunit interaction enough to prevent polymerization at room temperature at a concentration of 19 μM actin whereas removal of the side chains of both the N-terminal plug residues blocks F-actin formation.

The ability of three different agents to rescue polymerization of GG-actin offers additional insight into the forces that stabilize F-actin. The rescue of the polymerization defect of GG-actin by WT actin suggests that the WT actin provides sufficient normal cross-strand interaction per unit length of filament to permit stable helix formation in terms of the Holmes model. Binding of BeF_x to the filament, by virtue of stabilizing the filament in an ATP-like state, would enhance the ability of mutant ATP monomers to add to the ends of the filament and engage in the stronger monomer-monomer contacts characteristic of ATP- *versus* ADP-actin. Some residual stabilization might still be provided at 25 °C by interaction of Leu^{269} or the polypeptide backbone of the plug with the hydrophobic pocket, but a subsequent lowering of the temperature to 4 °C would decrease this residual interaction to the extent that a stable filament could no longer be maintained. Finally, phalloidin presumably promotes polymerization of pure GG-actin to an even greater extent than these other two methods by not only strengthening monomer-monomer contacts within a strand but also by providing an alternative form of cross-strand stabilization to replace that lost as a result of the disrupted plug-pocket interaction. This progression suggest that cross-strand stabilization involving the subdomain loop 3/4 plays an important part in actin helix formation.

An alternative explanation is that the GG mutation results in a monomer of lowered stability. This lowered stability could have any number of effects on the polymerizability of the monomer. The net Gibbs free energy change in transferring a monomer from solution to the polymer could be affected by structural changes influencing specific steps in the actin ATP exchange, hydrolysis, and product release steps. A less stable mutant monomer might be capable of entering into a polymer if enough wild-type monomers are present or if factors such as phalloidin provide product stabilization driving the reaction to completion.

Our results are consistent with all of these possibilities and detailed conclusions will require calorimetric and other data. However, the rescue of GG-actin polymerization by phalloidin, which binds only to polymers of actin, suggests that GG-actin can form polymers, perhaps only transiently, and that once stabilized, they serve as nuclei for further actin formation. If monomer denaturation prevented such interactions from occurring, phalloidin should have no effect. Second, our results (Fig. 9*C, curves 2* and *3*; Fig. 10, *B* and *C, curves 3* and *4*) showed that at 10 and 4 °C, a mixture of WT and GG-actin polymerizes to the same extent as that amount of WT actin alone. However, the mixture consistently appears to nucleate filament formation more rapidly than the WT actin alone. Thus, although at lower temperatures, the mutated loop is not hydrophobic enough to allow helix formation, GG-actin catalyzes the formation of filament nuclei by WT monomers. Such acceleration may reflect the ability of the mutant actin monomers to transiently form dimers or trimers in solution thereby leading to the formation of stable WT nuclei at an accelerated rate. Third, Schutt *et al.* argue that Leu^{269} and the β-carbon of D184 form part of the hydrophobic pocket that houses the hydrophobic side-chain of Leu^{267} leading to loop rigidity and monomer stabilization (15). However, our work shows that introduction of a negatively charged residue at position 269 (L269D) has no discernible effect on actin function *in vivo* or *in vitro*. Such a change should not only weaken the hydrophobic pocket in the monomer but might also be expected to further lower the stability of this region by electrostatic repulsion. Finally, additional studies from our laboratory[4] demonstrate that the GG mutation does, in fact, cause changes in the properties of the monomer, although there is no change in the K_d for ATP, and overall, these changes seem to convert the actin into a more F-actin monomer-like structure.

The hierarchy of effects associated with our various mutants is not totally consistent with predictions of the original Holmes model. The less severe effect associated with the V266D mutation in comparison with the L267D mutation appears to contradict the prediction that the N terminus of the plug should be the most sensitive in terms of dictating filament stability. The observations are more in agreement with a proposal by Tirion *et al.* (7) that the hydrophobic plug is not locked in the hydrophobic pocket as originally proposed by Holmes; *i.e.* the conformation of the hydrophobic plug can adapt to its environment to maximize available hydrophobic contacts and stabilize the actin filament. The GG mutation shows that a single hydrophobic residue at the C terminus of the plug is insufficient for polymerization. Separation of two hydrophobic residues by a charged residue would decrease the ability of the remaining hydrophobic side chains to participate in hydrophobic interactions with the opposing strand more than placement of a charge at either end of the plug. Further, separation of two adjoining hydrophobic residues by a space lowers the resulting interaction more than if the residues are contiguous. Lowering the temperature would decrease these interactions even further such that at some point, residual hydrophobic contacts would be insufficient to maintain helix integrity. The compatibility of GG-actin with yeast cell viability suggests that *in vivo*, actin filaments may be stabilized by actin binding proteins such as fimbrin and capping protein (44) in much the same way that phalloidin and BeF_x promote polymerization of GG-actin *in vitro*.

REFERENCES

1. Kabsch, W., Mannherz, H. G., Suck, D., Pai, E. F., and Holmes, K. C. (1990) *Nature* **347,** 37–44
2. Schutt, C. E., Myslik, J. C., Rozycki, M. D., Goonesekere, N. C. W., and Lindberg, U. (1993) *Nature* **365,** 810–816
3. McLaughlin P. J., Gooch, J. T., Mannherz, H. G., and Weeds, A. G. (1993) *Nature* **364,** 685–692
4. Holmes, K. C., Popp, D., Gebhard, W., and Kabsch, W. (1990) *Nature* **347,** 44–49
5. Lorenz, M., Popp, D., and Holmes, K. C. (1993) *J. Mol. Biol.* **234,** 826–836
6. Mendelson, R. A., and Morris, E. (1994) *J. Mol. Biol.* **240,** 138–154
7. Tirion, M. M., Ben-Avraham, D., Lorenz, M., and Holmes, K. C. (1995) *Biophys. J.* **68,** 5–12
8. Milligan, R. A., Whittaker, M., and Safer, D. (1990) *Nature* **348,** 217–221
9. Orlova, A., and Egelman, E. H. (1995a) *J. Mol. Biol.* **245,** 582–597
10. Orlova, A., and Egelman, E. H. (1995b) *J. Mol. Biol.* **245**, 598–607
11. Drubin, D. G., Jones, H. D., and Wertman, K. F. (1993) *Mol. Biol. Cell* **4,** 1277–1294
12. Hegri, G., Michel, H., Shabanowitz, J., Hunt, D. F., Chatterjie, N., Healy-Louie, G., and Elzinga, M. (1992) *Protein Sci.* **1,** 132–144
13. Moncman, C. L., Peng, I., and Winkelmann, D. A. (1993) *Cell Motil. Cytoskeleton* **25,** 73–86
14. Orlova, A., Yu, X., and Egelman, E. H. (1994) *Biophys. J.* **66,** 276–285
15. Schutt, E. C., Rozycki, M. D., Myslik, J. C., and Lindberg, U. (1995) *J. Struct. Biol.* **115,** 186–198
16. Schutt, E. C., Lindberg, U., Myslik, J. C., and Strauss, N. (1989) *J. Mol. Biol.* **209,** 735–746
17. Chen, X., Cook, R. K., and Rubenstein, P. A. (1993) *J. Cell Biol.* **123,** 1185–1195
18. Privalov, P. L., and Gill, S. J. (1988) *Adv. Protein Chem.* **39,** 191–234
19. Cook, R. K., Root, D., Miller, C., Reisler, E., and Rubenstein, P. A. (1993) *J. Biol. Chem.* **268,** 2410–2415
20. Sikorski, R., and Hieter, P. (1989) *Genetics* **122,** 19–27
21. Cook, R. K., Sheff, D. R., and Rubenstein, P. A. (1991) *J. Biol. Chem.* **266,** 16825–16833
22. Robzyk, K., and Kassir, Y. (1992) *Nucleic Acids Res.* **20,** 3790
23. Sherman, F. (1991) *Methods Enzymol.* **194,** 3–20

[4] Kuang, B., and Rubenstein, P. A. (1997) *J. Biol. Chem.* **272,** in press.

24. Pringle, J. R. (1991) *Methods Enzymol.* **194,** 732–734
25. Adams, A. E. M., and Pringle, J. R. (1991) *Methods Enzymol.* **194,** 729–731
26. Pringle, J. R., Adams, A. E. M., Drubin, D. G., and Haarer, B. K. (1991) *Methods Enzymol.* **194,** 565–601
27. Vida, T. A., and Emr, S. D. (1995) *J. Cell Biol.* **128,** 779–792
28. Nellen W., Donath, C., Moos, M., and Gallwitz, D. (1981) *J. Mol. Appl. Genet.* **1,** 239–244
29. Strzelecka-Golaszewska, H., Moraczewska, J., Khaitina, S. Y., and Mossakowska, M. (1993) *Eur. J. Biochem.* **211,** 731–742
30. Muhlrad, A., Cheung, P., Phan, B. C., Miller, C., and Reisler, E. (1994) *J. Biol. Chem.* **269,** 11852–11858
31. Chowdhury, S., Smith, K. W., and Gustin, M. C. (1992) *J. Cell Biol.* **118,** 561–571
32. Novick, P., and Botstein, D. (1985) *Cell* **40,** 405–416
33. Palmer, R. E., Sullivan, D. S., Huffaker, T., and Koshland, D. (1992) *J. Cell Biol.* **119,** 583–593
34. Adams, A. E. M., Johnson, D. I., Longnecker, R. M., Sloat, B. F., and Pringle, J. R. (1984) *J. Cell Biol.* **98,** 934–945
35. Cardenas, M. E., and Heitman, J. (1995) *EMBO J.* **14,** 5892–5907
36. Estes, J. E., Selden, L. A., Kinosian, H. J., and Gershman, L. C. (1992) *J. Muscle Res. Cell Motil.* **13,** 272–284
37. Carlier, M.-F., Pantaloni, D., and Korn, E. D. (1986) *J. Biol. Chem.* **261,** 10785–10792
38. Tobacman, L. S., and Korn, E. D. (1983) *J. Biol. Chem.* **258,** 3207–3214
39. Cooke, R. (1975) *Biochemistry* **14,** 3250–3256
40. Pollard, T. D. (1984) *J. Cell Biol.* **99,** 769–777
41. Carlier, M.-F., and Pantaloni, D. (1988) *J. Biol. Chem.* **263,** 817–825
42. Combeau, C., and Carlier, M.-F. (1988) *J. Biol. Chem.* **263,** 17429–17436
43. Orlova, A., and Egleman, E. H. (1992) *J. Mol. Biol.* **227,** 1043–1053
44. Karpova, T. S., Tatchell, K., and Cooper, J. A. (1995) *J. Cell Biol.* **131,** 1483–1493